

GLOBAL MAGNETOROTATIONAL INSTABILITY WITH INFLOW. II. THE NONLINEAR DEVELOPMENT OF AXISYMMETRIC WALL MODES

EVY KERSALÉ,¹ DAVID W. HUGHES,¹ GORDON I. OGILVIE,² AND STEVEN M. TOBIAS¹

Received 2005 August 12; accepted 2005 October 7

ABSTRACT

We investigate numerically the global, nonlinear behavior of magnetorotational instabilities in accretion disks by considering our previously formulated model of a cylindrical, dissipative disk with permeable boundaries. We extend the linear theory to follow the development of unstable, axisymmetric, magnetorotational modes into the nonlinear regime to determine the saturation mechanism. In each case parameters are chosen so that the most unstable mode is localized close to the inner boundary. We conduct an extensive parameter survey and find that the nonlinear behavior is mediated by the formation of a coherent radial jet that transports vertical magnetic flux within the disk. The mechanism for saturation depends critically on the strength of this jet. Different scenarios for saturation are explored in detail. The instability can either saturate in a nonlinear steady or oscillatory, non-Keplerian state, or relax back to a Keplerian state via the removal of flux from the disk by the jet.

Subject headings: accretion, accretion disks — instabilities — MHD

1. INTRODUCTION

The material in accretion disks orbits in the gravitational well produced by a central object, which can be, for instance, a forming star, a black hole or compact star in a binary system, or a supermassive black hole in the center of an active galaxy. The origin of the torque that produces accretion by removing angular momentum has been a long-standing issue in theoretical astrophysics. In the early 1990s Balbus & Hawley (1991) made a breakthrough by identifying, in the context of accretion disks, an instability mechanism responsible for angular momentum transport, previously studied by Velikhov (1959) and Chandrasekhar (1960). These “magnetorotational” instabilities (MRIs) develop linearly, on a dynamical timescale, in weakly magnetized rotating shearing flows. Following this seminal paper, the nonlinear evolution of MRIs and any associated dynamo action has been studied intensively through numerical computations (see, e.g., the review by Balbus & Hawley 1998). By considering first local, and then global models, simulations have gradually refined the modeling of physical processes acting in accretion disks (e.g., Hawley et al. 1995; Armitage 1998; Hawley 2000; Turner et al. 2002; Sano & Stone 2002). These informative studies, based on various levels of approximation, have shown the ability of MRIs to drive accretion via the production of strong turbulence. They do, however, leave a number of important questions unanswered. For instance, a deep understanding of the saturation mechanism of the instability is still lacking, and the nature of any dynamo action resulting from the MRI requires further investigation. In order to address these important issues, we consider it imperative to study models that possess certain key features. Global models, as opposed to local shearing box calculations, permit accretion and distinguish between inflows and outflows. Models that include dissipation explicitly allow a full understanding of the small-scale dynamics, and hence of the saturation mechanism of the MRI. The incorporation of boundary conditions that

permit global radial motions allows the development of a mean radial flow. Our understanding of the physical processes leading to the saturation of MRIs and dynamo growth in accretion disks will benefit from a progressive increase in the complexity of the models considered.

In Kersalé et al. (2004, hereafter Paper I) we formulated the simplest model that incorporates all of the above desirable features, the details of which are summarized in § 2, and, using this model, presented the linear theory for the global stability of dissipative magnetized accretion disks in Keplerian rotation. It is worth elaborating here on the philosophy underlying the construction of this model. There are two possible approaches to the computational modeling of turbulent processes in astrophysical fluid dynamics. One is formally to neglect all dissipative terms on the grounds that these are small. However, *all* numerical schemes contain truncation errors, which are either dissipative or dispersive in nature. Therefore, results obtained in this manner will in fact be influenced by dissipation; moreover, the form of the dissipation is unknown (depending on the numerical scheme employed) and is resolution dependent. The other approach, which is the one we have adopted in constructing our model, is to include the dissipative processes explicitly. This has the advantage that the small-scale dynamics of the flow are correctly calculated. Furthermore, with present-day computational resources it is possible to explore genuinely turbulent regimes.

In Paper I we demonstrated that, in agreement with local studies, there is a class of unstable MRI modes with eigenfunctions that spread over the whole disk and reach their maxima away from the boundaries (“body” modes). We also found that with boundary conditions that permit net radial flows, another class of modes, localized in the vicinity of the boundaries, is also unstable. We term these “wall” modes, since they correspond to a maximum of the perturbation of the radial velocity on the boundaries. The wall modes developing at the inner radial boundary were found to be the most unstable of *all* possible modes since they grow at the place where the most free energy can be extracted from the differential rotation. Moreover, they are unstable over a much wider range of azimuthal wavenumbers than that of body modes, although this range shrinks when an azimuthal component of the magnetic field of strength comparable to that of the poloidal field is present. We also demonstrated that

¹ Department of Applied Mathematics, University of Leeds, Leeds LS2 9JT, UK; kersale@maths.leeds.ac.uk, dwh@maths.leeds.ac.uk, smt@maths.leeds.ac.uk.

² Department of Applied Mathematics and Theoretical Physics, Centre for Mathematical Sciences, University of Cambridge, Wilberforce Road, Cambridge CB3 0WA, UK; g.i.ogilvie@damtp.cam.ac.uk.

the local properties of the MRI (i.e., when the curvature of the disk is neglected) are recovered in our global model within the limit of small spatial scale perturbations. Finally, in Paper I we stressed the extreme sensitivity of wall modes to the boundary conditions, and explained how particular care is needed in order to avoid feeding the unstable modes artificially.

Although the linear theory of MRIs is of prime importance in elucidating the instability mechanism and identifying the regimes in parameter space in which instability can occur, a complete understanding of MRIs can only be attained by investigating their nonlinear evolution. The very few analytical nonlinear results that exist have all been obtained in the approximation of a two-dimensional local Cartesian geometry. Goodman & Xu (1994) showed, for instance, that in the absence of dissipation the linear, incompressible MRI modes are also solutions of the nonlinear equations. In addition, they investigated the stability of these solutions and their possible disruption via parasitic instabilities. Making use of asymptotic expansions, Knobloch & Julien (2005) found a fully nonlinear, stable, equilibrated state of a dissipative system in a regime of parameters relevant for accretion disks. However, such analytical results, although important, cannot capture all the complexity of the nonlinear evolution of the MRI. In order to obtain significant insights into the nonlinear dynamics of global MRIs it is therefore imperative also to adopt the complementary approach of solving the governing equations by numerical simulation.

In this paper we build on the results of Paper I to investigate the evolution of wall modes into the nonlinear regime. The most unstable linear modes are axisymmetric, and thus, in keeping with the philosophy outlined above of gradually extending the complexity of our model, we restrict our attention in this paper to the *axisymmetric* nonlinear evolution of the disk. Within this framework we are able to address some of the issues of the nonlinear saturation of the MRI but cannot, of course, investigate any aspects of dynamo action. Section 2 describes the global model of a dissipative accretion disk with permeable boundaries. The description of the numerical code to solve the equations of incompressible magnetohydrodynamics (MHD) is contained in § 3. The main results are explained in § 4; we discuss the properties of the coherent structures that emerge in the nonlinear regime, address the issue of the instability suppression, and describe the cyclic evolution of the system and its possible relaxation to a nontrivial steady state. We also comment on the nature of the transport of mass for each of the nonlinear evolutions considered. The conclusions and implications of our results are presented in § 5.

2. SETUP OF THE MODEL

We adopt the simplest model, as discussed in detail in Paper I and illustrated in Figure 1, that retains all the essential features required for the linear and nonlinear study of the MRI: a differentially rotating, cylindrical annulus of finite thickness, composed of an incompressible, resistive, viscous plasma threaded by a magnetic field. We do not attempt to model the entire accretion disk, but restrict our attention to an annular section—localized far from the central object and external regions—of a larger, extended disk. The distinguishing feature of our model is that the boundary conditions are formulated so as to allow a radial flow, both in the basic state and in the subsequent development of the instability. As shown below, the flow in the basic state is proportional to the viscosity, which we choose to be small, whereas the radial flow driven by the instability is not constrained by dissipation. We do not take into account the influence of more refined effects such as compressibility, self-gravitation,

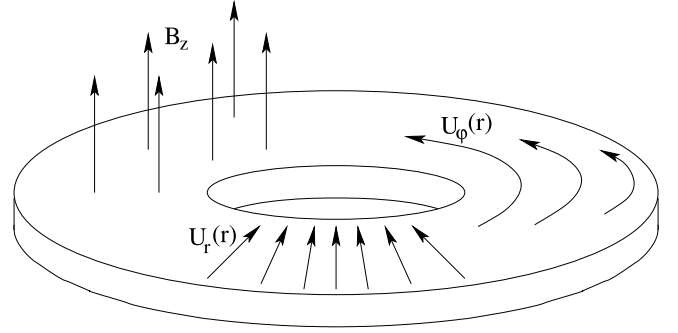


FIG. 1.—Sketch of our model of a slim, magnetized, dissipative accretion disk. A gravitational potential creates an azimuthal differentially rotating flow, which in turn drives an accretion flow through viscous effects.

radiation, the Hall effect, or vertical stratification, all of which, though possibly important, are not the concern of the current work.

Under the assumptions of our model, the governing equations for the velocity field $\mathbf{U} = (U_r, U_\phi, U_z)$ and magnetic field $\mathbf{B} = (B_r, B_\phi, B_z)$ are those of incompressible, constant density MHD, which can be written as

$$\left(\frac{\partial}{\partial t} + \mathbf{U} \cdot \nabla\right) \mathbf{U} = -\nabla\Phi - \nabla\Pi + \mathbf{B} \cdot \nabla\mathbf{B} + \nu\nabla^2\mathbf{U}, \quad (1)$$

$$\left(\frac{\partial}{\partial t} + \mathbf{U} \cdot \nabla\right) \mathbf{B} = \mathbf{B} \cdot \nabla\mathbf{U} + \eta\nabla^2\mathbf{B}, \quad (2)$$

$$\nabla \cdot \mathbf{B} = \nabla \cdot \mathbf{U} = 0, \quad (3)$$

where Φ is the external gravitational potential acting on the disk, Π is the total pressure (thermal plus magnetic) divided by the density, ν is the kinematic viscosity of the plasma, and η is electrical resistivity. The magnetic field is measured in terms of the Alfvén speed.

The basic state consists of an axisymmetric, uniformly magnetized ($B_z = \text{const}$), Keplerian flow ($U_\phi \propto 1/\sqrt{r}$), and is taken to be invariant in the vertical direction. For such rotating shearing flows, a viscous torque acting within the disk removes angular momentum and produces an accretion flow, $U_r \propto -\nu/r$. We stress again that we choose ν to be small, so that the radial flow of the basic state, together with its associated mass flux, is correspondingly small. In order to accommodate this flow—and any nonlinear accretion flows—we are required to consider nontrivial choices of boundary conditions. In particular, the radial boundaries must be permeable in order to allow global radial motions. The conditions that we choose to impose at both radial boundaries are

$$\frac{\partial}{\partial r}(\sqrt{r}U_\phi) = \frac{\partial U_z}{\partial r} = 0, \quad \frac{\partial}{\partial r}(rB_\phi) = \frac{\partial B_z}{\partial r} = 0, \quad (4)$$

together with

$$\nabla \cdot \mathbf{U} = \nabla \cdot \mathbf{B} = 0 \quad \text{and} \quad \Pi = \text{constant}. \quad (5)$$

An inevitable consequence of this choice is the occurrence of an advective flux of magnetic field out of (or into) the disk; hence, there is no conservation of magnetic flux within the disk. For simplicity we also impose periodicity in the vertical direction. These conditions have been chosen to be as neutral as possible while enforcing fundamental features of the model such as Keplerian rotation and a small radial pressure gradient. The

importance of formulating these boundary conditions correctly, together with the consequences of different choices of boundary conditions, are discussed in detail in Paper I.

3. NUMERICAL METHOD

In order to compute the nonlinear evolution of unstable wall modes, we have developed a semi-implicit, two-dimensional, pseudospectral numerical code to solve the non-ideal incompressible MHD equations in an annulus, in such a way that dissipative and resistive processes are treated explicitly and do not rely on numerical effects. A detailed discussion of the numerical techniques involved in the code can be found in E. Kersalé (2006, in preparation). The general framework underlying our numerical approach has previously been discussed in the literature and has been widely used, for instance in the context of convection and dynamos in spherical geometry (e.g., Glatzmaier 1984; Clune et al. 1999). Nevertheless, the geometry of our model and the boundary conditions that we implement modify some important features of the numerical scheme and raise different technical issues.

The use of spectral methods for partial differentiation in space benefits from their fast convergence properties (Canuto et al. 1988). As discussed in Paper I, the linear theory of unstable wall modes suggests the development of boundary layers. For this reason, we utilized a radial expansion in Chebyshev polynomials, expressed at the Chebyshev-Gauss-Lobatto collocation points, which increases the resolution in the vicinity of the boundaries. In the vertical direction, the periodicity of the computational domain suggests a Fourier decomposition. The dependent variables \mathbf{U} , \mathbf{B} and Π are thus expanded in the basis of trial functions as

$$X(r, z) = \sum_{l,k} \mathcal{X}_{lk} T_l(s) e^{ikz}, \quad (6)$$

where $T_l(s) = \cos(l \cos^{-1} s)$ are the Chebyshev polynomials, and s is a linear function of radius.

To integrate the equations in time we make use of a semi-implicit numerical scheme, Crank-Nicolson and fourth-order Adams-Bashforth (both with adaptive time step) for the linear and nonlinear terms, respectively. The discretization of the equations of incompressible MHD gives a set of implicit equations that can be inverted using standard direct methods, such as LU decomposition, or iterative methods, such as the conjugate gradient method. The values of \mathbf{U} , \mathbf{B} and Π , after $n + 1$ iterations in time, are then obtained by solving the system

$$\begin{aligned} \nabla^2 \Gamma^{n+1} &= \nabla \cdot \mathcal{N}_u^n \\ (\mathcal{I} - \Theta \delta t \mathcal{L}) \mathbf{U}^{n+1} + \nabla \Gamma^{n+1} &= \mathcal{N}_u^n + [\mathcal{I} + (1 - \Theta) \delta t \mathcal{L}] \mathbf{U}^n, \\ (\mathcal{I} - \Theta \delta t \mathcal{L}) \tilde{\mathbf{B}}^{n+1} &= \mathcal{N}_b^n + [\mathcal{I} + (1 - \Theta) \delta t \mathcal{L}] \mathbf{B}^n, \end{aligned}$$

where $\Theta \in [0, 1]$, $\Gamma = \delta t \Pi$, $\mathcal{L} = \nu \nabla^2$, \mathcal{I} is the identity matrix, and \mathcal{N} represents the nonlinear terms (given by the fourth order Adams-Bashforth algorithm). As described, this algorithm cannot preserve the solenoidal property of \mathbf{B}^n (i.e., $\nabla \cdot \tilde{\mathbf{B}}^{n+1} \neq 0$). In order to recover this fundamental feature of the magnetic field, we employ a projection method whereby $\tilde{\mathbf{B}}^{n+1}$ is projected onto a divergence-free vector field in order to ensure that \mathbf{B}^{n+1} is solenoidal:

$$\mathbf{B}^{n+1} = \tilde{\mathbf{B}}^{n+1} - \nabla \Psi \quad \text{with} \quad \nabla^2 \Psi = \nabla \cdot \tilde{\mathbf{B}}^{n+1}. \quad (7)$$

The code is pseudospectral, meaning that the nonlinear terms are evaluated not in Chebyshev-Fourier space but in configu-

ration space. Indeed, this approach benefits from fast Fourier transform algorithms (Cooley & Tukey 1965; Frigo & Johnson 1998), which require fewer floating point operations than convolution algorithms. We also make use of the properties of the trial functions to perform all the other computations in spectral space; for instance, first- and second-order spatial derivatives can be expressed as simple multiplications in z and recurrence relations in r . This approach is straightforward for the Fourier components but requires further algebraic developments for Chebyshev polynomials because of the nature of the equations in cylindrical coordinates (Gottlieb & Orszag 1977; Coutsias et al. 1996). The development of the discrete differential operators involved in the Crank-Nicolson scheme, in particular, has required a lot of attention. The vertical boundary conditions are automatically satisfied by the trial functions (Galerkin method), while the Dirichlet, Neumann, and Robin radial boundary conditions give simple linear relations between the Chebyshev expansion coefficients. These auxiliary equations, derived from boundary conditions, have to be solved in spectral space together with the discretized equations of MHD (τ method).

4. NONLINEAR EVOLUTION

The nonlinear evolution of axisymmetric wall modes is governed by five parameters: the viscosity ν , the magnetic diffusivity η , the imposed magnetic field strength, the ratio of the outer to inner radii, and the vertical extent of the domain. Since a complete investigation of the full five-dimensional parameter space is not feasible, it is important to concentrate on varying only those parameters that we believe may lead to qualitative changes in the dynamics. To this end we have therefore restricted our investigations to the case of $\nu = \eta$. We have employed resolutions up to 128×128 and have chosen ν (and η) to be as small as possible, compatible with the resolution. This leads to Reynolds numbers (flow and magnetic) of the order of several hundred; thus the timescale for dissipative processes to act far exceeds the orbital period of the disk. The other parameter values are chosen such that, according to linear theory, only one mode is unstable. Within these confines we have performed an extensive, systematic survey of the dynamical behavior resulting from variation of the parameters. We have identified four different possible routes for the nonlinear evolution. In the following subsections we explore each of these in depth via illustrative examples.

In each numerical experiment we trigger the instability by the superposition of random, small-amplitude perturbations to the equilibrium azimuthal velocity field. After an initial transient, an exponentially growing wall mode emerges, localized close to the inner boundary, and with a growth rate in good agreement with the predictions of linear theory. Our choice of parameters makes this the *only* possible growing mode.

The governing equations and boundary conditions are non-dimensionalized by scaling lengths with the inner radius and times with the Keplerian orbital period at the inner radius. We denote the five dimensionless parameters that govern the problem by: ν , the dimensionless viscosity; η , the dimensionless magnetic diffusivity; B_0 , the strength of the initially imposed magnetic field; R_2 , the outer radius; and H , the vertical extent of the domain.

4.1. Suppression of the Instability

We consider first a model with $R_2 = 2$, $H = 1/2$, $B_0 = 6.3 \times 10^{-2}$ and $\nu = \eta = 3.5 \times 10^{-3}$. The complete evolution, from the initial (unstable) equilibrium through to the final (stable) configuration, is encapsulated in Figure 2. The initial transient ($t \lesssim 1$ and hence not discernible in the figure) is followed by a period of exponential growth ($1 \lesssim t \lesssim 410$) governed by

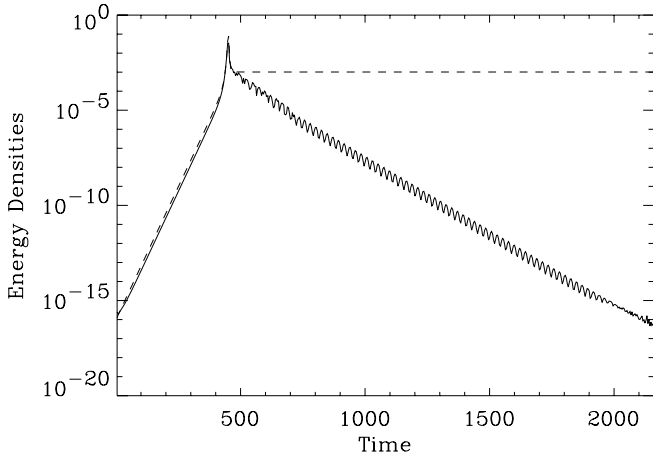


FIG. 2.—Evolution of the kinetic (*solid line*) and magnetic (*dashed line*) energy densities of the perturbations for a model with $R_2 = 2$, $B_0 = 6.3 \times 10^{-2}$, and $\nu = \eta = 3.5 \times 10^{-3}$. The linear growth rate, in which the unit of time is the Keplerian orbital period at the inner boundary, is $\gamma \simeq 3.2 \times 10^{-2}$. Note that the magnetic perturbation in the final state corresponds to a reduction of the total magnetic energy.

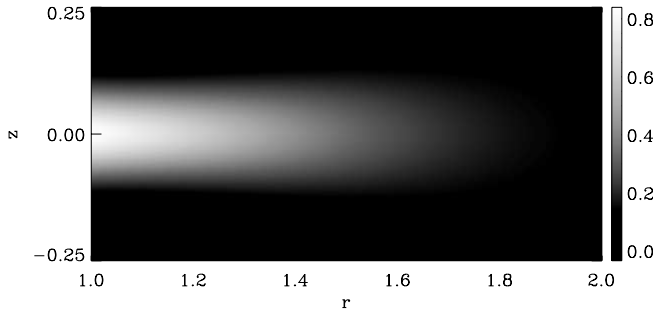


FIG. 3a

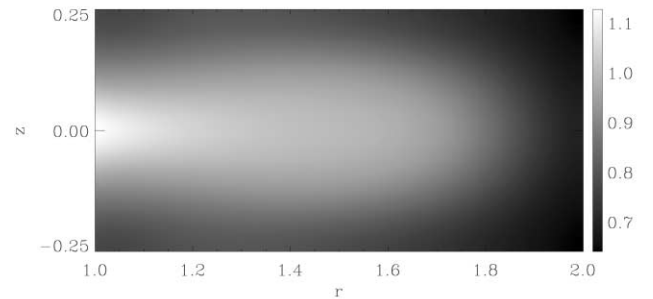


FIG. 3b

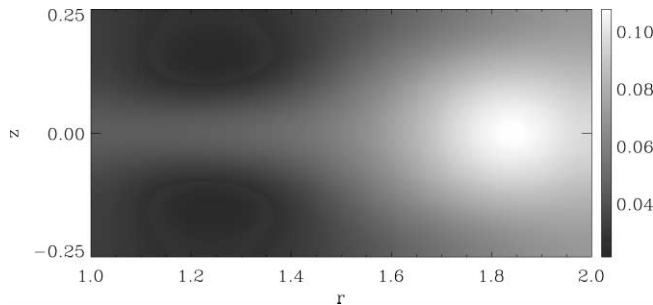


FIG. 3c

FIG. 3.—Snapshot of the nonlinear evolution of an unstable wall mode at $t = 448$ for the same model as in Fig. 2, showing (a) radial velocity, (b) azimuthal velocity, and (c) vertical magnetic field.

linear theory. At the end of this period nonlinear effects become important, and there is a brief interval during which rapid readjustment of the disk takes place ($410 \lesssim t \lesssim 480$). There follows a final stage ($t \gtrsim 500$) during which the disk relaxes to a new equilibrium.

When nonlinear effects become important, the structure of the radial velocity evolves into a coherent jetlike structure propagating throughout the disk; a snapshot of U_r , U_φ , and B_z at $t = 448$ is shown in Figure 3. (The coherent structures appear vertically centered, since we can arbitrarily choose the random phase of the perturbation of the linearly unstable mode to be zero.) The vertical thickness of the structure is controlled by viscosity, with its extent decreasing as the viscosity decreases. Eventually, the amplitude of the radial jet becomes comparable with that of the azimuthal velocity. Furthermore, at this stage, the angular velocity profile is drastically modified, becoming strongly non-Keplerian, as shown in Figure 3b.

Figure 4 exhibits the dynamics in the interval of rapid nonlinear adjustment. Figure 4a shows, as a function of time, the radial mass flux \dot{M} , defined by

$$\dot{M} = 2\pi r \rho \int_{-H/2}^{H/2} U_r dz, \quad (8)$$

where $\dot{M} > 0$ corresponds to an outward radial mass flux. Owing to the assumptions of incompressibility and vertical

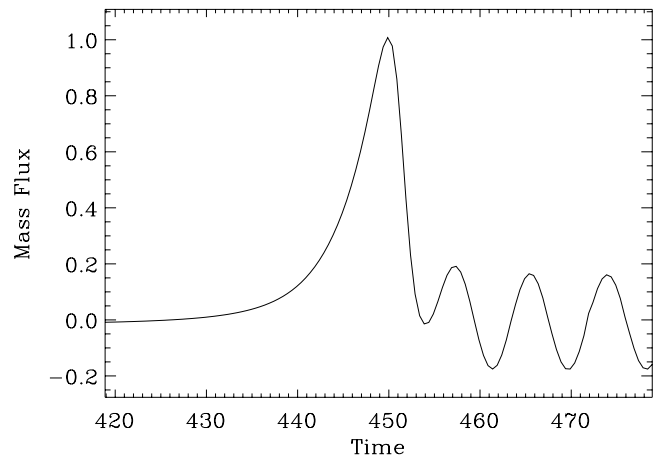


FIG. 4a

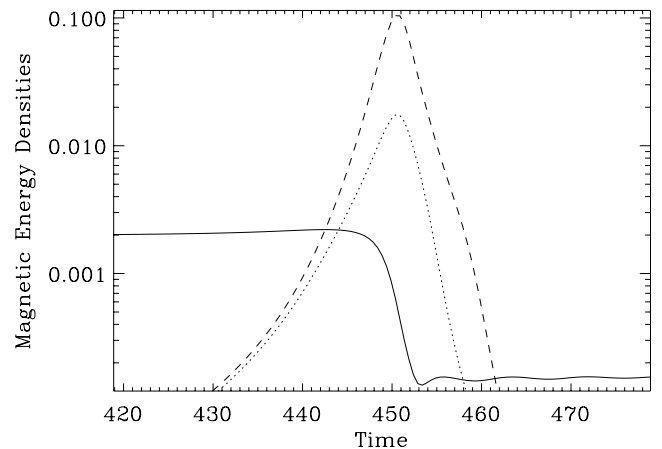


FIG. 4b

FIG. 4.—Same model as in Fig. 2, showing evolution of (a) the radial mass flux (the accretion rate) and (b) the energy densities of the vertical (*solid line*), radial (*dotted line*), and azimuthal (*dashed line*) components of the magnetic field.

periodicity, this quantity does not depend on radius and, in the absence of nonlinear effects, is driven solely by the viscous torque. Figure 4a shows the formation of a net radial outflow, and Figure 4b the simultaneous, superexponential growth of the three components of the magnetic field. Of particular note are the strong radial and azimuthal components, induced by shears in the radial and azimuthal velocities. Figure 3c exhibits the outward transport of the vertical magnetic field by the coherent radial flow. In this model the jet produced nonlinearly is sufficiently powerful to advect a significant fraction of the vertical magnetic field out of the computational domain. This leads to an abrupt and significant drop in the energy of the vertical field, as shown in Figure 4b. As discussed in Paper I, the reduction in field strength in the presence of resistivity leads to the suppression of the MRI in the disk. The radial jet immediately shuts off and the azimuthal and radial magnetic fields, relying on the MRI, rapidly vanish. It is worth reiterating that the timescale for the suppression of the MRI is very short compared to that of the initial exponential growth.

Immediately after the instability switches itself off, the azimuthal velocity is far from Keplerian, leading to epicyclic oscillations of the whole disk; these global motions are not prevented by the radial boundary conditions. Figure 2 shows that these radial oscillations are damped on a dissipative timescale, the system eventually relaxing to a new equilibrium. The flow returns to its initial Keplerian state, with an inflow produced by the viscous torque and a uniform vertical magnetic field. The amplitude of the field has decreased compared with its initial value in such a way that the system has become linearly stable. Recall from Paper I that, in dissipative systems, reduction of magnetic energy can lead to stabilizing MRIs.

We have found that this mechanism of nonlinear suppression occurs for a wide range of values of the dissipation coefficients, provided that the initial vertical magnetic field is strong enough (i.e., that B_0 is comparable to or larger than the field that triggers the most unstable linear mode). In this experiment, the MRI is controlled by either the radial extent of the computational domain or the strength of the wall mode; a sufficiently powerful jet is required to expel enough vertical magnetic flux out of a narrow annulus.

4.2. Cyclic Evolution

The example in § 4.1 showed how the MRI could be switched off, self-consistently, by the removal of magnetic flux from the disk by a strong radial jet. It is of interest therefore to investigate models for which flux cannot so easily be removed. Two ways by which this might be achieved are: (1) increasing the radial extent of the disk, and (2) decreasing the vigor of the instability and, consequently, the strength of the associated jet.

Initially we have computed the evolution of an unstable wall mode in a radially extended system with $R_2 = 4$, with the other parameters as in the example discussed in § 4.1. As in the previous example, after the growth of the linear wall mode a radial outflow transports vertical magnetic flux from the inner part of the disk outward. However, in contrast to the case with $R_2 = 2$, the flux is not expelled but remains within the disk. Recall that the disk is most unstable at the inner boundary; hence, removal of flux from the inner part of the disk leads to stabilization of the linear instability. Furthermore, the energetic jet gives rise to large-amplitude radial oscillations of the disk, as shown in Figure 5a. Dissipative effects eventually damp these oscillations and the system relaxes essentially to its initial kinetic and magnetic states (see Fig. 5b). More explicitly, once the MRI is inhibited by a deficit of vertical magnetic field in the

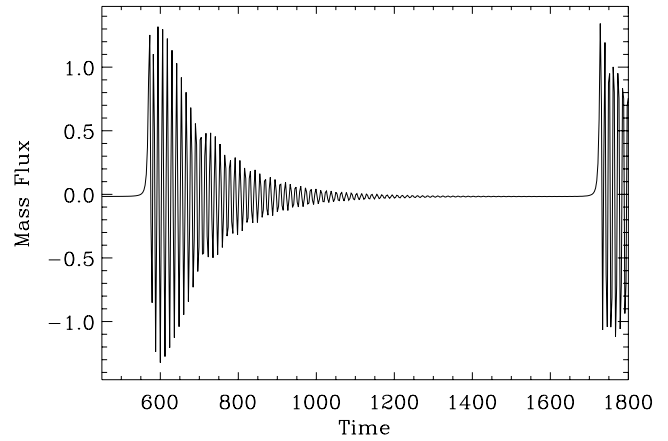


FIG. 5a

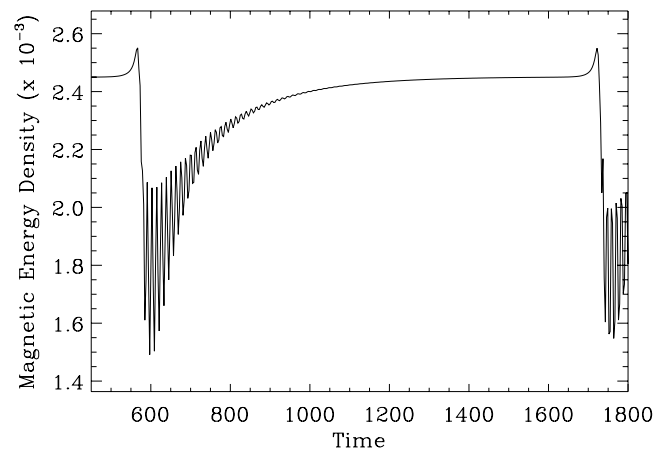


FIG. 5b

FIG. 5.—Evolution of (a) the radial mass flux and (b) the energy density of the vertical magnetic field, for a model with $R_2 = 4$, $B_0 = 7 \times 10^{-2}$, $\nu = \eta = 3.5 \times 10^{-3}$; the linear growth rate is $\gamma \approx 2.7 \times 10^{-2}$.

inner region, accretion sets in and brings the magnetic flux, which has accumulated at large radii, back toward the center of the disk. In our model this is a slow (dissipative) process, since accretion is driven solely by the viscous stress. After this “recovery” phase the system has returned to its unstable initial state. The whole sequence of events—linear growth, rapid nonlinear readjustment, and linear dissipative decay—is then repeated indefinitely. The cyclic nature of the evolution is clearly illustrated by Figure 6, which shows the long-term behavior of the energy densities of the perturbations. For these parameter values the system is therefore acting as a relaxation oscillator.

With a view to preventing the removal of magnetic flux from the disk, we revisit the case of a narrow disk ($R_2 = 2$) but with a weaker MRI, triggered by a reduced initial magnetic field, $B_0 = 5 \times 10^{-2}$. Here the jet produced is not powerful enough to expel the magnetic flux out of the computational domain. This type of behavior occurs for field strengths B_0 that are small compared with that of the most unstable linear mode for the specified viscosity and resistivity. For this case, the initial nonlinear phase leads to a *partial* loss of magnetic flux that is not sufficient to prevent accretion from rebuilding a magnetically unstable configuration (see Fig. 7a). As shown by Figure 8, the kinetic and magnetic energy perturbations are then reamplified until their growth is suppressed by the action of the radial jet. Repetition of this process leads to cyclical, and indeed eventually

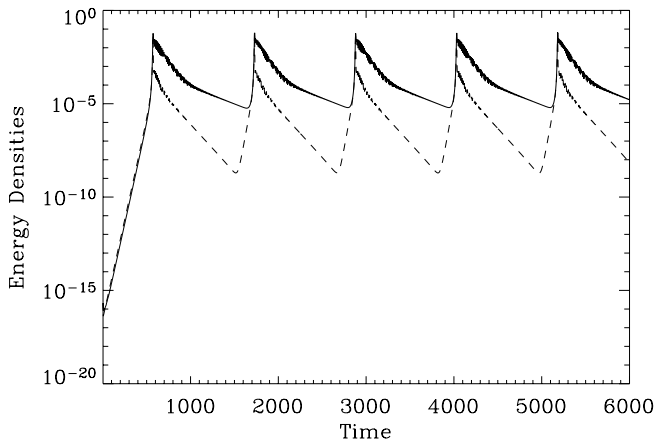


FIG. 6.—Same model as in Fig. 5, evolution of the kinetic (*solid line*) and magnetic (*dashed line*) energy densities of the perturbations.

periodic, behavior. However, in contrast to the case discussed immediately above, the evolution cannot be split into distinct linear and nonlinear phases, but is fully nonlinear throughout. This is exemplified by Figure 8, in which it can be seen that, except for the *initial* period of exponential growth, there is no

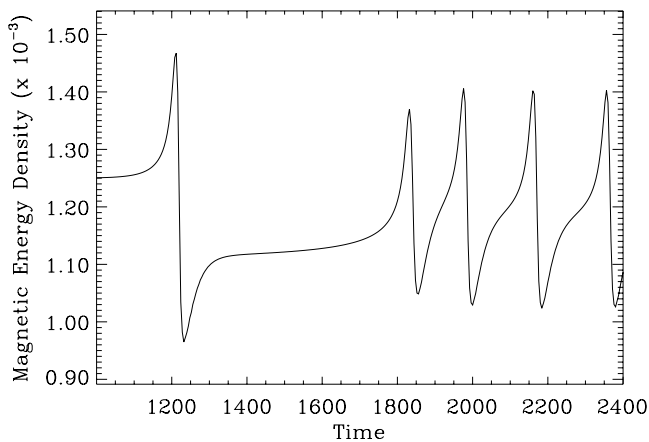


FIG. 7a

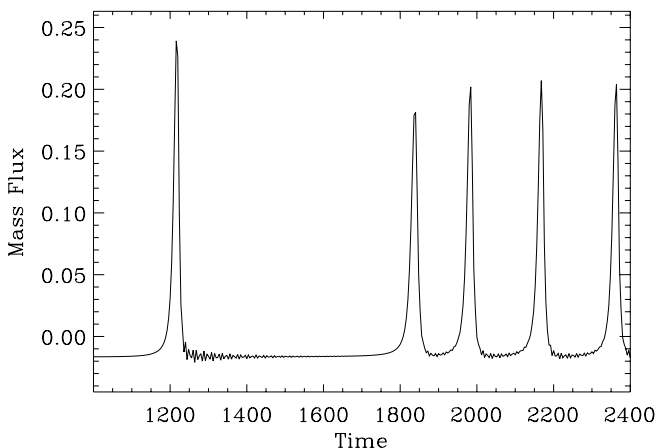


FIG. 7b

FIG. 7.—Evolution of (a) the energy density of the vertical magnetic field and (b) the radial mass flux for a model with $R_2 = 2$, $B_0 = 5 \times 10^{-2}$, $\nu = \eta = 3.5 \times 10^{-3}$; the linear growth rate is $\gamma \simeq 1.1 \times 10^{-2}$.

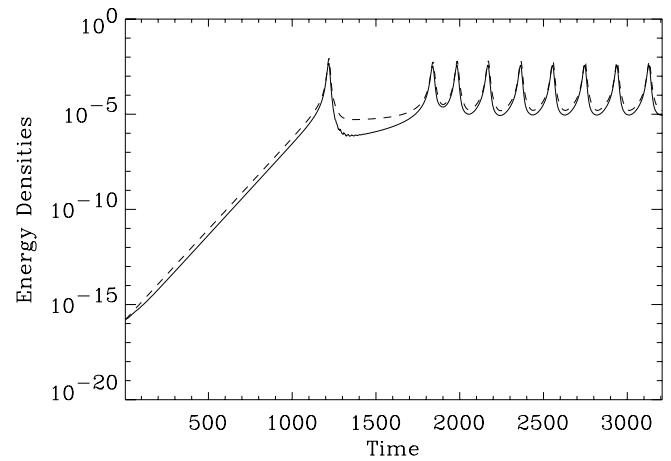


FIG. 8.—Same model as in Fig. 7, showing evolution of the kinetic (*solid line*) and magnetic (*dashed line*) energy densities of the perturbations.

strictly linear regime. For the case shown in Figure 6, the nonlinear stresses become negligible during the relaxation phase; for the evolution portrayed in Figure 8 the nonlinear stresses are always significant, and oscillate about the value of the viscous stress. Thus, whereas in the former the timescale between bursts is determined by dissipation, in the latter this interval, although long dynamically, is shorter than a dissipative timescale, being controlled by both dissipative and nonlinear effects. In the example portrayed in Figure 8 the mass carried by the nonlinear jet is significantly diminished in comparison with the two cases discussed earlier, and hence no large-amplitude oscillations of the system occur (cf. Figs. 4a and 5a with Fig. 7b). The evolution of the radial flow and vertical magnetic field over one typical cycle is shown in Figure 9; the generation of the jet, which displaces vertical magnetic flux toward the outer boundary, is followed by a phase where accretion redistributes the field uniformly across the disk.

4.3. Evolution to a Nontrivial Steady State

In all of the numerical experiments described above, the formation of a strong radial jet has played the key role in regulating the dynamical behavior of the flow and field. For the case discussed in § 4.1, this process is particularly violent, leading to the expulsion of the vertical magnetic field from the domain and the complete suppression of the instability. The system returns to a Keplerian flow with a weaker uniform magnetic field. If, however, the domain is radially extended, as for the first case in § 4.2, flux is only moved outward, but not totally expelled; this leads to relaxation oscillations of the form shown in Figure 6. A weaker magnetic field, as in the second case in § 4.2, leads to nonlinear oscillations, as shown in Figure 8. Here we investigate the evolution from a yet weaker field, for which we expect a less pronounced radial jet with a reduced capacity for “cleaning” the inner portion of the disk of the vertical magnetic field responsible for the MRI.

We consider the evolution of the system with a weak initial field, $B_0 = 3.5 \times 10^{-2}$, and with $R_2 = 2$ and $\nu = \eta = 3 \times 10^{-3}$ (note that we have had to decrease the diffusivities in order to destabilize the system with such a weak field). Figure 10a demonstrates that, after the linear regime (characterized by a vertically sinusoidal eigenfunction, with the net flux of mass driven solely by the viscous stress, and not by the MRI), a radial jet emerges. However, by comparison with the other examples, the jet is weak, with a mass flux of only the same order of magnitude as the

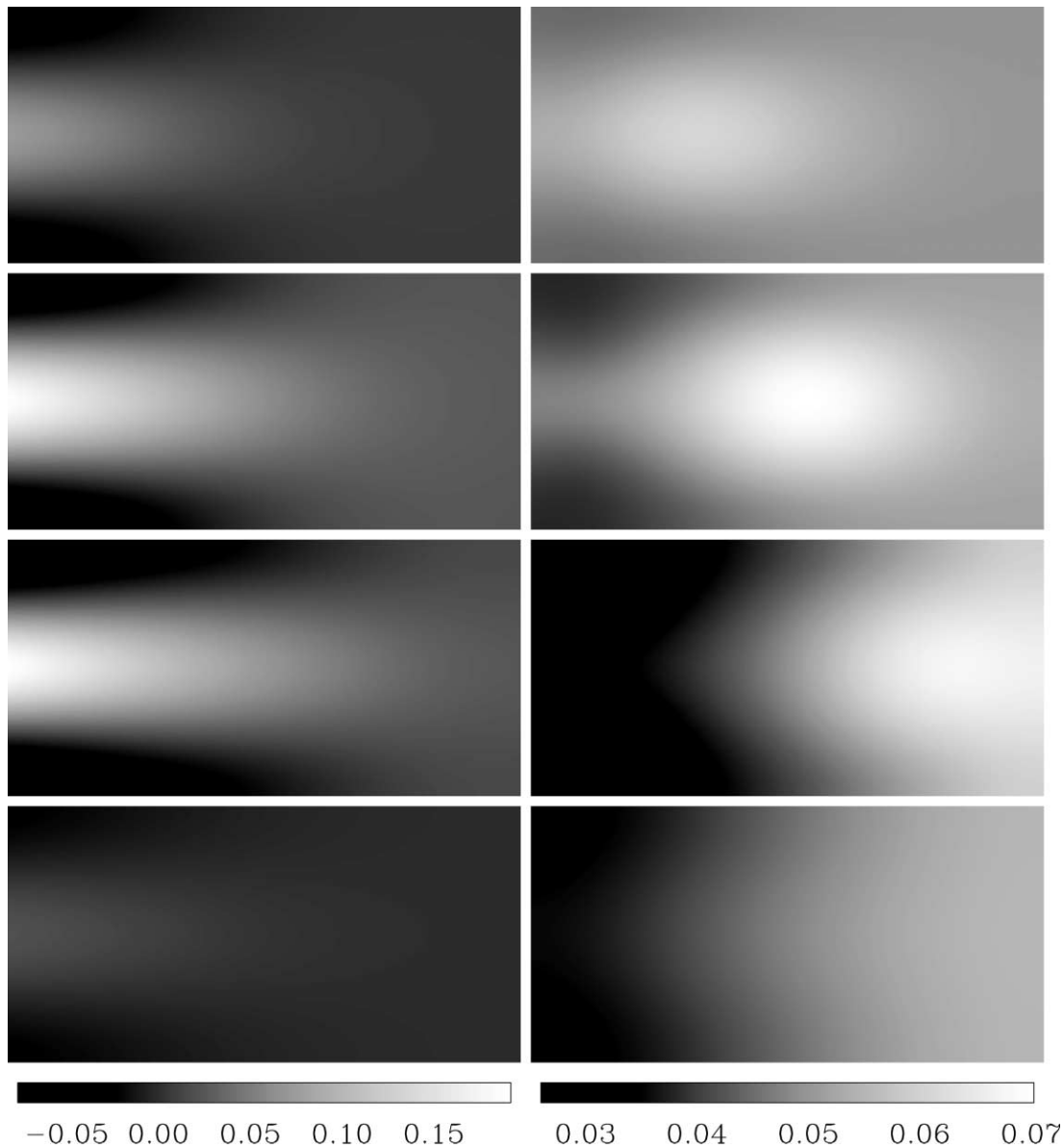


FIG. 9.—Same model as in Fig. 7, showing maps of the radial velocity (*left*) and the vertical magnetic field (*right*) at different times (*increasing downward*) during a cycle.

accretion rate of the initial Keplerian state (cf. Figs. 4*a*, 5*a*, and 7*b* with Fig. 10*a*). This weak jet is not powerful enough to suppress the instability. Indeed, after a transient phase of successive adjustments, the system relaxes on a dissipative timescale to a new stable, steady equilibrium. In this nonlinear state, for which the vertical magnetic energy has increased (see Fig. 10*b*), the MRI still acts to drive a net outward flux of material. Figure 11 shows the structure of the radial velocity, azimuthal velocity, and vertical magnetic field in the final steady state, which is characterized by a balance between the outward radial jet and the inward accretion flow (see Fig. 11*a*). The jet is fairly weak and so the flow is only mildly non-Keplerian (Fig. 11*b*). Figure 11*c* shows the structure of the vertical magnetic field; although its maximum lies at $r \approx 1.7$, there is sufficient field at the inner radii to drive the MRI.

4.4. Radial Mass Flux

A feature of our nonlinear solutions that deserves discussion concerns the direction of the radial mass transport. For the

example of § 4.1, both the initial and final states are Keplerian and have an inward radial mass flux. However, as shown in Figure 4*a*, the radial jet leads to an interval during which the flux is *outward*, with a magnitude greatly in excess of the viscous-driven flux of the Keplerian state. The epicyclic oscillations of the whole disk provide no net transport of radial mass. A similar scenario is observed for the examples of § 4.2, with the strong radial jet leading to an outward transport of mass. For these systems, which eventually become periodic, the time average of the radial mass flux is positive. For the example discussed in § 4.3 the final steady state has an outward mass flux, as clearly seen in Figure 10*a*. It is noteworthy therefore that, at least within the constraints of our model, the addition of a magnetic field to a Keplerian flow, and the subsequent development of MRIs, does not lead to enhanced accretion but instead to an outward radial transport of mass.

This transport can be understood by examining the evolution of angular momentum in the disk. Suppose we split the velocity field into mean and fluctuating parts with respect to vertical averaging.

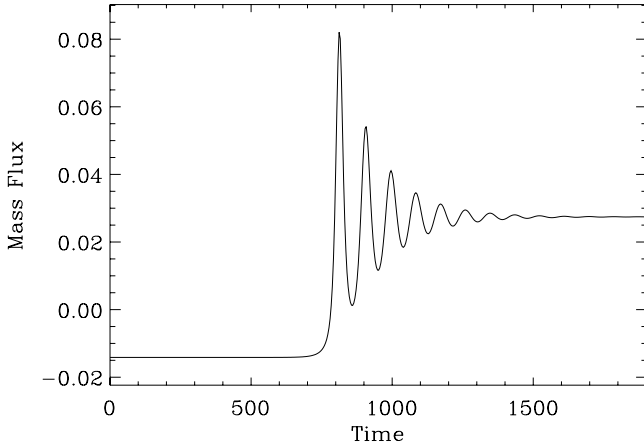


FIG. 10a

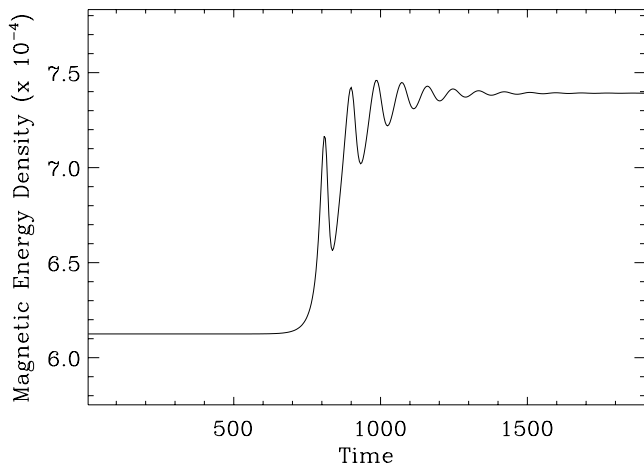


FIG. 10b

FIG. 10.—Evolution of (a) the energy density of the vertical magnetic field and (b) the radial mass flux, for a model with $R_2 = 2$, $B_0 = 3.5 \times 10^{-2}$, $\nu = \eta = 3 \times 10^{-3}$; the linear growth rate is $\gamma \simeq 1.7 \times 10^{-2}$.

Then $\mathbf{U}(r, z, t) = \bar{\mathbf{U}}(r, t) + \mathbf{U}'(r, z, t)$, with $\int_0^H \mathbf{U}' dz = 0$. Vertical integration of the angular momentum equation gives

$$\frac{\partial J}{\partial t} + F \frac{\partial(r\bar{U}_\varphi)}{\partial r} = -\frac{\partial G}{\partial r}, \quad (9)$$

where $F = 2\pi r \rho H \bar{U}_r$ is the radial mass flux, $J = 2\pi r \rho H r \bar{U}_\varphi$ is the angular momentum per unit radius, and

$$G = 2\pi \rho r^2 \int_{-H/2}^{H/2} \left[U'_r U'_\varphi - B_r B_\varphi - \nu r \frac{\partial}{\partial r} \left(\frac{\bar{U}_\varphi}{r} \right) \right] dz \quad (10)$$

is the torque contributed by Reynolds, Maxwell, and viscous stresses. It should be noted that, as a consequence of incompressibility, $\partial_r F = 0$.

In the nonlinear state G is positive, dominated by positive contributions from the Reynolds and Maxwell stresses. Since the MRI develops at the inner radius, G is clearly a function of position, such that $\partial_r G < 0$. Hence, if the $\partial_r J$ term is negligible (because the disk remains close to Keplerian on account of the radial force balance), then F is determined by (minus) the ratio of the torque gradient to the mean angular momentum gradient

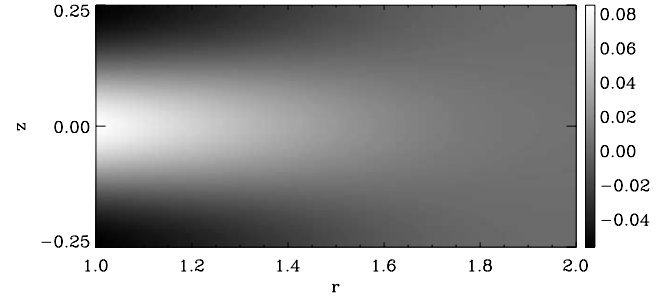


FIG. 11a

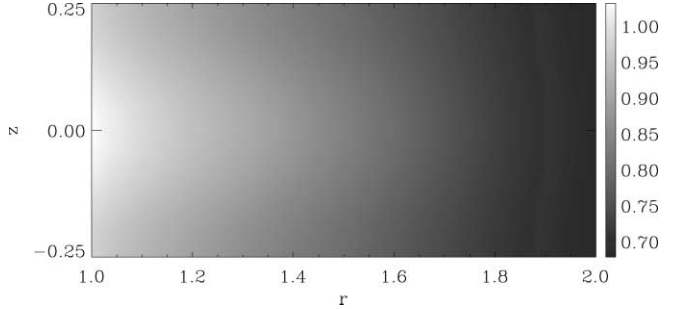


FIG. 11b

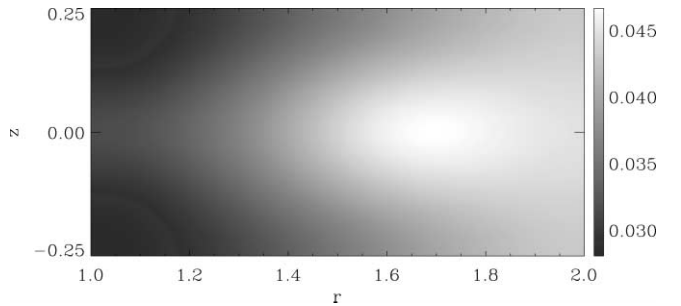


FIG. 11c

FIG. 11.—Same model as in Fig. 10, showing snapshot of the nontrivial steady state; (a) radial velocity; (b) azimuthal velocity, and (c) vertical magnetic field.

(which should be close to the Keplerian value). Hence, an outward mass flux is driven. The annulus is gaining angular momentum as a result of stresses acting at the inner boundary, so an outward motion is driven to accommodate the extra angular momentum. This is what happens in the outer parts of accretion disks with free outer boundaries, and also in accretion disks where the central star exerts a torque on the disk. So, even though the Reynolds, Maxwell, and viscous stresses may have the “correct” sign, the direction of the radial flow depends on more subtle effects that have to do with the radial inhomogeneity of the system. This property illustrates the difficulty of reproducing some global features of accretion flows within a computational domain.

In the standard theory of thin accretion disks (e.g., Pringle 1981) the $\partial_r J$ term would be dropped for the reason given above. For the evolution discussed in § 4.3 the final state is steady (i.e., $\partial_t J = 0$), and the torque balance is as described above. For the cases considered in §§ 4.1 and 4.2, the nonlinear states obtained are time dependent, and $\partial_r J$ is not negligible. The radial mass flux is time dependent; it is outward when the nonlinear stresses dominate and inward when these diminish, the flux then being driven by the linear (viscous) stress.

5. CONCLUSION AND DISCUSSION

In Paper I we addressed the linear theory of MRIs in magnetized, rotating shearing flows in a disk with permeable boundaries. Such a system permits the development of global radial motions. In the present paper, we have extended the study of the most unstable MRI modes (namely the axisymmetric wall modes) into the nonlinear regime. Making use of the numerical code described in § 3, we have performed a survey over a three-dimensional parameter space of the nonlinear evolution of isolated, linearly unstable wall modes. We find that for all values of B_0 and ν ($=\eta$) considered, all with values comparable with those used in § 4, the nonlinear development of wall modes does not lead to turbulence; instead, it produces coherent structures leading to either a cyclic evolution of the system or a relaxation to a new trivial or nontrivial steady state. One of the main features of the nonlinear evolution is the formation of radial jets, which have the ability to transport vertical magnetic flux across the computational domain; depending on the strength of the jet (determined by a combination of the dissipation coefficients and the amplitude of the initial magnetic field), the system exhibits different possible final states. In certain cases the jet is so powerful that it evacuates enough magnetic flux out of the computational domain to reach a new stable Keplerian steady state (§ 4.1). For parameters that lead to radial jets of lower energy the system exhibits periodic behavior (§ 4.2), first with cycles showing successive phases of fast nonlinear evolution followed by slow linear relaxation, and then, for yet weaker jets, cycles controlled entirely by the nonlinear dynamics. In the case of the weakest jets (§ 4.3), the timescale of the nonlinear processes is sufficiently long to permit a smooth reorganization of the system and its relaxation to a nontrivial steady state in which both the MRI and the accretion play an important role in the equilibration. As noted in § 4.4, the nonlinear equilibration of the MRIs leads to an outward radial mass flux.

The radial jets that are responsible for the redistribution of the magnetic flux can be contrasted with the well-known channel flow solutions observed in two-dimensional local (shearing box) numerical simulations (Hawley & Balbus 1992). Both solutions exhibit strong radial flows driven by the presence of a net poloidal magnetic field. However, while the channel flows take the form of exponentially growing solutions to the fully nonlinear system, with a sinusoidal vertical dependence that fills the vertical extent of the domain and no radial dependence, the radial jets are saturated solutions to the nonlinear equations and exhibit nontrivial vertical and radial structure. Furthermore, the radial jets develop as a consequence of the radial inhomogeneity of the system, whereas there is no such inhomogeneity in the local shearing box. Finally, in contrast to the channel flow solutions, the radial jets drive net transport (of mass and magnetic flux) through the system.

In general, MHD or hydrodynamic instabilities saturate either by enhancing dissipation through the generation of turbulence or by modifying the driving mechanism for the instability, or a combination of both. In local periodic models (e.g., Hawley et al. 1995) enhancement of the dissipation via turbulent interactions is the only available mechanism for saturating the MRI. Modification of the driving mechanism by amendment of the shear profile has been investigated by Knobloch & Julien (2005). They found that in this case the MRI first evolves nonlinearly on a fast (dynamical) timescale, and then relaxes on a slow (dissipative) timescale to a saturated steady state. Our model allows not only saturation via these mechanisms but also the additional possibility of modification of the driving via a redistribution of the magnetic flux. In § 4.1 this mechanism is clearly crucial for the saturation of the instability, whereas in § 4.3 it goes hand in hand with the modification of the shear profile.

We have already emphasized that viscosity plays a key role in determining the width of the radial jets emerging in the nonlinear regime, with lower dissipation leading to stronger vertical confinement. (This is consistent with the tendency of MRIs to develop smaller scales vertically than radially [Hawley & Balbus 1992].) Hence, for Reynolds numbers higher than those considered here, we expect narrower jets, and the possible development of Kelvin-Helmholtz instabilities. Even in two dimensions such a process would lead to the disruption of the jet and a more disordered evolution of the system. We also conjecture that the coherent jets are destabilized by nonaxisymmetric perturbations, consistent with the findings of a number of nonlinear simulations. Three-dimensional computations of the evolution of our global model will certainly produce more complicated, spatially less coherent turbulent flows. It is conceivable, in contrast to the axisymmetric evolutions considered here, that such MRI-driven three-dimensional MHD turbulence will lead to an *inward* mass flux, as usually found in the inner parts of numerical models of accretion. The investigation of the three-dimensional nonlinear evolution of MRIs in disks that permit net radial flows is therefore an outstanding and important problem. We regard the stable two-dimensional structures identified in this paper as possible building blocks for such three-dimensional flows. For instance, three-dimensional chaotic flows may well exhibit, in a statistical sense, features of the simpler nonlinear stable solutions found in two dimensions. In this context, it is of interest to note that the characteristic spike-shaped variations in energy density, seen for example in Figure 8, are a typical feature of nonlinear turbulent three-dimensional models (e.g., Sano & Inutsuka 2001).

The authors acknowledge financial support from PPARC under grant number PPA/G/S/2000/00147. We are grateful to N. O. Weiss for helpful discussions.

REFERENCES

- Armitage, P. J. 1998, *ApJ*, 501, 189
 Balbus, S. A., & Hawley, J. F. 1991, *ApJ*, 376, 214
 ———. 1998, *Rev. Mod. Phys.*, 70, 1
 Canuto, C., Hussaini, M. Y., Quateroni, A., & Zang, T. A. 1988, *Spectral Methods in Fluid Dynamics* (New York: Springer)
 Chandrasekhar, S. 1960, *Proc. Natl. Acad. Sci.*, 46, 253
 Clune, T. C., Elliott, J. R., Miesch, M. S., Toomre, J., & Glatzmaier, G. A. 1999, *Parallel Comput.*, 25, 361
 Cooley, J. W., & Tukey, J. W. 1965, *Math. Comput.*, 19, 297
 Coutsias, E. A., Hagstrom, T., & Torres, D. 1996, *Math. Comput.*, 65, 611
 Frigo, M., & Johnson, S. G. 1998, *Proc. IEEE*, 3, 1381
 Glatzmaier, G. A. 1984, *J. Comput. Phys.*, 55, 461
 Goodman, J., & Xu, G. 1994, *ApJ*, 432, 213
 Gottlieb, D., & Orszag, S. A. 1977, *Numerical Analysis of Spectral Methods: Theory and Applications* (Philadelphia: SIAM)
 Hawley, J. F. 2000, *ApJ*, 528, 462
 Hawley, J. F., & Balbus, S. A. 1992, *ApJ*, 400, 595
 Hawley, J. F., Gammie, C. F., & Balbus, S. A. 1995, *ApJ*, 440, 742
 Kersalé, E., Hughes, D. W., Ogilvie, G. I., Tobias, S. M., & Weiss, N. O. 2004, *ApJ*, 602, 892
 Knobloch, E., & Julien, K. 2005, *Phys. Fluids*, 17, 9
 Pringle, J. E. 1981, *ARA&A*, 19, 137
 Sano, T., & Inutsuka, S. 2001, *ApJ*, 561, L179
 Sano, T., & Stone, J. M. 2002, *ApJ*, 577, 534
 Turner, N. J., Stone, J. M., & Sano, T. 2002, *ApJ*, 566, 148
 Velikhov, E. P. 1959, *Sov. Phys.-JETP Lett.*, 36, 995